Biogeosciences, 11, 4459–4476, 2014
www.biogeosciences.net/11/4459/2014/
doi:10.5194/bg-11-4459-2014

Biogeosciences Open Access

Methyl iodide production in the open ocean

I. Stemmler[1,3], **I. Hense**[1], **B. Quack**[2], **and E. Maier-Reimer**[3]

[1]Institute for Hydrobiology and Fisheries Science, University of Hamburg, CEN, Hamburg, Germany
[2]Geomar, Helmholtz Centre for Ocean Research, Kiel, Germany
[3]Max Planck Institute for Meteorology, Hamburg, Germany

Correspondence to: I. Stemmler (irene.stemmler@zmaw.de)

Received: 16 October 2013 – Published in Biogeosciences Discuss.: 8 November 2013
Revised: 2 July 2014 – Accepted: 8 July 2014 – Published: 22 August 2014

Abstract. Production pathways of the prominent volatile organic halogen compound methyl iodide (CH_3I) are not fully understood. Based on observations, production of CH_3I via photochemical degradation of organic material *or* via phytoplankton production has been proposed. Additional insights could not be gained from correlations between observed biological and environmental variables or from biogeochemical modeling to identify unambiguously the source of methyl iodide. In this study, we aim to address this question of source mechanisms with a three-dimensional global ocean general circulation model including biogeochemistry (MPIOM–HAMOCC (MPIOM – Max Planck Institute Ocean Model HAMOCC – HAMburg Ocean Carbon Cycle model)) by carrying out a series of sensitivity experiments. The simulated fields are compared with a newly available global data set. Simulated distribution patterns and emissions of CH_3I differ largely for the two different production pathways. The evaluation of our model results with observations shows that, on the global scale, observed surface concentrations of CH_3I can be best explained by the photochemical production pathway. Our results further emphasize that correlations between CH_3I and abiotic or biotic factors do not necessarily provide meaningful insights concerning the source of origin. Overall, we find a net global annual CH_3I air–sea flux that ranges between 70 and 260 $Gg\,yr^{-1}$. On the global scale, the ocean acts as a net source of methyl iodide for the atmosphere, though in some regions in boreal winter, fluxes are of the opposite direction (from the atmosphere to the ocean).

1 Introduction

Methyl iodide (CH_3I) is an organic halogen of natural origin. Following emission from the ocean (or land), it is photolyzed within days into reactive iodine species that affect the oxidative capacity of the atmosphere (e.g., via ozone depletion) (Chameides and Davis, 1980; Solomon et al., 1994; Rattigan et al., 1997; Vogt et al., 1999; Carpenter, 2003). CH_3I is ubiquitously detected in water and air in the marine boundary layer (e.g., Singh et al., 1983; Happell and Wallace, 1996; Chuck et al., 2005; Smythe-Wright et al., 2006; Butler et al., 2007; Fuhlbrügge et al., 2013). The strength of the CH_3I source to the atmosphere is estimated using two different methods. It is either derived from extrapolating fluxes diagnosed from concentrations measured during ship cruises (e.g., Moore and Groszko, 1999; Chuck et al., 2005; Butler et al., 2007; Jones et al., 2010; Ziska et al., 2013) or by analyzing oceanic source and sink processes (e.g., Manley and De La Cuesta, 1997; Bell et al., 2002; Carpenter, 2003; Richter and Wallace, 2004; Youn et al., 2010). In this regard, several marine macroalgae have been identified as CH_3I producers (Gschwend et al., 1985; Nightingale et al., 1995; Itoh et al., 1997; Giese et al., 1999; Carpenter et al., 2000), and are thought to be the dominant source in the coastal ocean. In the open ocean, there is evidence of several production pathways: production through photochemical degradation of organic matter (e.g., Moore and Zafiriou, 1994; Richter and Wallace, 2004), production by marine biota (e.g., Smythe-Wright et al., 2006; Amachi, 2008; Karlsson et al., 2008; Brownell et al., 2010), or substitution when dust contacts seawater containing iodide or when marine water vapor condenses on dust containing iodide (Williams et al., 2007). A common method for deducing production pathways is from

the covariation of CH_3I concentrations and abiotic and biotic proxy parameters. Observed CH_3I concentrations in seawater and marine air were correlated with phytoplankton biomass (Smythe-Wright et al., 2006), phytoplankton pigment concentrations (Abrahamsson et al., 2004; Chuck et al., 2005; Wang et al., 2009; Lai et al., 2011), temperatures (Rasmussen et al., 1982; Happell and Wallace, 1996; Yokouchi et al., 2001; Chuck et al., 2005; Wang et al., 2009), and radiation (Happell and Wallace, 1996; Chuck et al., 2005; Wang et al., 2009). Most of these studies suggested that CH_3I is produced via the biological or photochemical production pathway. Laboratory studies identify several phytoplankton species (e.g., *Nitzschia, Phaeocystis, Prochlorococcus, Synechococcus, Emiliania, Thalassiosira, Phaeodactylum*) (Moore and Tokarczyk, 1993; Hughes et al., 2006; Smythe-Wright et al., 2006; Brownell et al., 2010; Toda and Itoh, 2011) as CH_3I producers. Additionally, heterotrophic, non-photosynthesizing bacteria (Manley and Dastoor, 1988; Manley, 1994; Amachi et al., 2001; Fuse et al., 2003; Amachi, 2008) decomposing detrital particles (Hughes et al., 2008) have been proposed as constituting significant biological sources of CH_3I. The photochemical production pathway has also been observed in laboratory experiments (e.g., Richter and Wallace, 2004). These methods, i.e., the extrapolation from ship-based measurements to global sources or emissions, and the extrapolation from laboratory to natural conditions, include inherent uncertainties. On the one hand, it is questionable whether phytoplankton cultivated under laboratory conditions behaves like in the open ocean. On the other hand, measurements from field campaigns only reflect snapshots, and it is unclear whether they can be used to identify possible production pathways.

Numerical models can help to reduce these uncertainties. They can be used to test different findings on production and to extrapolate consistently (based on process parameterizations) in space and time. Previous model studies have been conducted, but they also show contradictory evidence of a photochemical or direct biological production pathway. Bell et al. (2002) and Youn et al. (2010) studied CH_3I originating from natural sources using a global atmospheric chemistry-transport model coupled to a mixed layer ocean model. In the work of Bell et al. (2002) (and in Youn et al. (2010), who adopted the same parameterization), model and observation agreed best when only photochemical sources were considered instead of biological production. In a recent model study with a one-dimensional water-column model, Stemmler et al. (2013) assessed the relevance of different production pathways for representing observed CH_3I profiles in the tropical Atlantic Ocean. The results indicated, in contrast to Bell et al. (2002), that production by phytoplankton dominated the vertical CH_3I profile at Cape Verde. Effects of horizontal and vertical advection, however, were neglected. Previous global model studies were based on relatively few observations, because they could not make use of the recently established global data set for organic halogens (Ziska et al., 2013). It is thus still unclear whether surface concentrations might or might not be best explained by direct biological or photochemical production. In the current study, we use the methyl iodide module within a global oceanic general circulation model, MPIOM–HAMOCC (Marsland et al., 2003; Ilyina et al., 2013), and the global data set of CH_3I observations (Ziska et al., 2013) to re-address the question of different CH_3I production pathways. We also aim to analyze relationships between CH_3I concentrations and biotic as well as abiotic variables in a similar way as is done with field measurements, to assess the interpretability of these correlations. Furthermore, we derive sea–air fluxes to investigate possible differences in CH_3I emissions due to different sources; the results will be compared with published emission estimates.

2 Material and methods

2.1 Model description

Methyl iodide modeling was performed with the MPIOM (Max Planck Institute Ocean Model) (Marsland et al., 2003) ocean general circulation model coupled to the HAMOCC5.2 (Six and Maier-Reimer, 1996; Ilyina et al., 2013) marine carbon cycle model and the CH_3I module presented in Stemmler et al. (2013). Methyl iodide cycling includes production, degradation, air–sea gas exchange, diffusion and advection. Two production mechanisms are resolved: direct biological production by phytoplankton, and photochemical production by radical recombination between methyl groups and iodine atoms. Biological production of CH_3I follows phytoplankton growth using either a constant or variable phytoplankton-to-methyl-iodide production ratio. Photochemical production is parameterized linearly to radiation and a dissolved organic carbon concentration. CH_3I degradation includes nucleophilic substitution with chloride, hydrolysis, and photolysis. Degradation processes are described as first-order kinetics with temperature-dependent rates taken from the literature (Elliott and Rowland, 1993, 1995; Rattigan et al., 1997). Gas exchange is calculated from the two-film model using an annual mean climatology of atmospheric concentrations (Ziska et al. (2013), robust fit interpolation method, see Sect. 2.3 on the data basis), the Schmidt number (Moore and Groszko, 1999), and a transfer velocity (Nightingale et al., 2000). A detailed description of process parameterizations and the chemical properties of CH_3I can be found in Stemmler et al. (2013).

2.2 Model setup

For this study, MPIOM version 1.5.0 was run at a horizontal resolution of approximately 1.5° (i.e., GR15L40). It uses a curvilinear grid, with the North Pole shifted over Greenland. The model resolves 40 vertical levels of varying depths, with a higher resolution in the upper, sun-lit ocean, where primary production (PP) takes place.

Table 1. Model experiments defined by the production pathway considered. Experiments are called "Opt" to be consistent with Stemmler et al. (2013), who derived the CH_3I production rates from a parameter optimization.

Production pathway/	Biological		Photochemical		Mixed	
experiment ID	Opt1	Opt2	Opt3	Opt4	Opt134	Opt24
"Normal" biological prod.	+				+	
"Stressed" biological prod.		+				+
Photochemical prod. from SLDOC			+		+	
Photochemical prod. from RDOC				+	+	+

Based on our insights from previous model experiments in which the production rates were optimized to best fit observed concentrations (Stemmler et al., 2013), we performed the following experiments (Table 1).

Opt1. "Normal" biological production: Stemmler et al. (2013) demonstrated that in the model experiment with optimized parameters for biological production, the best agreement with observed profiles of CH_3I could be achieved. In particular, the model was able to reproduce the low surface concentration and a pronounced subsurface maximum. We therefore adopt this experiment in which CH_3I is produced during phytoplankton growth using a constant production ratio.

Opt2. "Stressed" biological production: Stemmler et al. (2013) showed that the consideration of enhanced production by physiologically stressed phytoplankton (i.e., the picocyanobacteria species *Prochlorococcus*), as suggested by Hughes et al. (2011), did not improve the model performance. Due to several uncertainties discussed in Stemmler et al. (2013), the importance of this mechanism can not be excluded; we therefore consider this production pathway. In this experiment, the CH_3I production rate varies in space and time, depending on nutrient availability.

Opt3. Photochemical production from semi-labile dissolved organic carbon (SLDOC): Bell et al. (2002) state in their model study that best agreement between simulated and observed CH_3I surface concentrations is achieved when photochemical production using SLDOC is taken into account; we therefore follow their approach. In this experiment, CH_3I production is linearly coupled to light and dissolved organic carbon concentration, which is provided by HAMOCC.

Opt4. Photochemical production from a constant surface DOC pool: model sensitivity experiments with photochemical production of SLDOC or refractory dissolved organic carbon (RDOC) did not reveal significant differences (Stemmler et al., 2013) at Cape Verde. It is not obvious that this is true on a global scale; we therefore also consider this production pathway. In this experiment, CH_3I production is linearly coupled to light.

Opt134. "Normal" biological production and both photochemical production pathways: it is expected that in reality, both biological and photochemical production occur simultaneously; this experiment therefore represents combined production.

Opt24. "Stressed" biological production and photochemical production from refractory DOC: this combination of source processes was chosen as it became clear from Opt1 to Opt4 that "stressed" biological production and photochemical production from RDOC best represent observations in surface seawater on the global scale (see Sect. 3.3 and Table 3). The experiment considers "stressed" biological production, with the ratio between CH_3I production and phytoplankton growth $k_{PP} \in [0.1232, 200]$ mmol CH_3I (kmolP)$^{-1}$ and photochemical production from RDOC with the photochemical production rate $k_{photo} = 2.8 \times 10^{-7}$ m^2 mmol CH_3I (kmolP)$^{-1}$ W^{-1} s^{-1}.

All rates for CH_3I production are identical to the ones used in Stemmler et al. (2013): no new parameter optimization was performed. For all experiments, the ocean model was restarted from an 840-year spin-up under preindustrial conditions, i.e., using a constant atmospheric CO_2 concentration of 278 ppm. A subsequent chemical spin-up run over 50 years starting from a constant CH_3I concentration of 1 pmol L^{-1} was performed to ensure steady-state conditions. The ocean model was forced with Ocean Model Intercomparison Project data (OMIP forcing) (Röske, 2006), which is a daily mean climatology based on ECMWF (European Centre for Medium-Range Weather Forecasts) Re-Analyses (ERA) data (Gibson et al., 1997). To test the sensitivity towards the atmospheric forcing, one experiment (Opt4) was repeated with transient (1959–1964) NCEP (National Centers for Environmental Prediction) 6 h data (Behringer and Xue, 2004). Model results presented here are from a one-year simulation that followed the spin-up.

Table 2. Global production, loss, emissions, and inventory.

Production pathway	Biological		Photochemical		Mixed	
	Opt1	Opt2	Opt3	Opt4	Opt134	Opt24
Production [Gg yr^{-1}]	427.23	407.49	125.49	217.14	348.27	305.97
% biological	100	100			0.2	29
% photochemical SLDOC			100		28	
% photochemical RDOC				100	72	71
Net emission [Gg yr^{-1}]	256.62	218.55	69.09	101.52	170.61	149.46
Loss [Gg yr^{-1}]	141.00	180.48	53.58	109.98	164.97	148.05
Inventory [Gg]	22.56	12.69	5.64	12.69	14.10	11.28

2.3 Observations

CH_3I data are extracted from the HalOcAt (Halocarbons in the Ocean and Atmosphere) database (https://halocat.geomar.de/, Ziska et al., 2013). HalOcAt was initiated in May 2009 as an initiative of SOLAS Project Integration as part of COST Action 735 (an EU-funded networking tool) and SOPRAN (http://sopran.pangaea.de/). Currently the database contains about 200 data sets with a total of 55 400 oceanic and 476 000 atmospheric concentrations from all depth and height levels of 19 different halocarbon compounds (mainly very short-lived brominated and iodinated trace gases) from the years 1989 to 2011. Only data from the upper 20 m of the ocean are used here to evaluate model performance (Fig. 1). Generally, observed data from a particular month are compared to modeled monthly means. The exact origin of the individual data can be identified from the supplemental information (SI) in Ziska et al. (2013). Among other sources listed in Ziska et al. (2013), observations from air and seawater of the Atlantic are from Butler et al. (2007), Chuck et al. (2005), Jones et al. (2010), Schall et al (1997), and Wang et al. (2009), of the Pacific from Butler et al. (2007) and Yokouchi et al. (2008), of the Southern Ocean from Abrahamsson et al. (2004), Butler et al. (2007), Chuck et al. (2005), and Yokouchi et al. (2008), and of other ocean regions from Archer et al. (2007), Orlikowska and Schulz-Bull (2009), and Yokouchi et al. (2008).

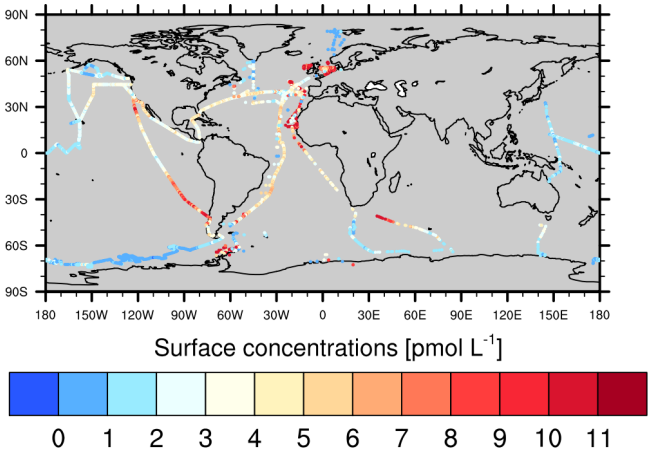

Figure 1. Observed surface methyl iodide concentration (pmol L^{-1}).

3 Results

3.1 Simulated mean fields

Biological methyl iodide production in the model is proportional to primary production. Two experiments were performed, one with "normal" biological production, in which the ratio between CH_3I production and primary production is kept constant (Opt1), the other with a varying ratio (Opt2), which is high in oligotrophic oceans and low where phytoplankton growth is rarely nutrient limited. In total, approximately 400 Gg of CH_3I are produced by phytoplankton within one year, but more than 94 % is lost via degradation and outgassing (Table 2).

In Opt1, the spatial and temporal patterns of CH_3I production mirror the ones of primary production (Fig. 1a). The highest production throughout the year occurs in regions of equatorial upwelling, and seasonally in the Southern Ocean (in boreal fall and winter) or the North Pacific and Atlantic (in boreal spring and summer). Strong outgassing and degradation lead to a relatively short overall residence time τ ($\tau = \frac{\text{inventory}}{\text{sinks}}$) in the ocean of approximately 20 days. Consequently, in most oceanic regions, CH_3I does not accumulate, and the spatial patterns resemble the ones of primary production (Figs. 3a and 4a). By contrast, CH_3I concentrations in the Arctic Ocean are high in summer and fall despite low primary production (not shown). The reasons for this are small losses, i.e., reduced outgassing in summer when the wind speed is low, and slow chemical reactions (hydrolysis, nucleophylic substitution) at cold temperatures. Furthermore, methyl iodide production occurs within the mixed layer. Deepening of the mixed layer in windy seasons leads to a dilution of concentrations, which is not compensated for

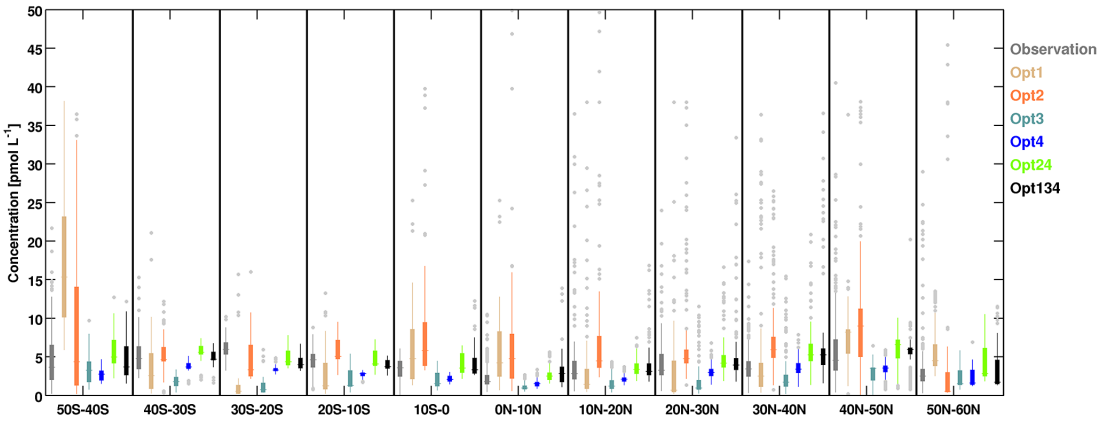

Figure 2. Box–whisker plot of simulated and observed surface ocean CH_3I concentrations (pmol L^{-1}). Box widths are determined by the 25 and 75 % percentiles of data within each 10-degree latitude box; outliers (gray) are located outside 1.5 times the differences of the percentiles; the middle line of each box shows the median. Simulated concentrations are averaged over 1-degree boxes around the locations of the observations. Different colors denote different experiments; observations are shown in dark gray.

by production, and which thus results in a longer residence time.

In Opt2, the presence of stressed picocyanobacteria cells leading to enhanced CH_3I production is simulated by implementing the ratio between CH_3I production and growth k_{PP} as a function of nutrient availability (Stemmler et al., 2013). In this way, k_{PP} is spatially and temporally variable, with maxima in the subtropical gyres and minima in nutrient-rich regions such as upwelling regimes (Fig. 4b). The inhomogeneous production rate leads to different CH_3I distribution patterns compared to primary production (Figs. 3b and 4a). Though concentration maxima at the Equator persist, more CH_3I is produced and remains in the subtropical gyres, whereas CH_3I in the Southern Ocean is reduced. These changes in the spatial distribution of CH_3I production are in line with changes in the relative importance of the loss processes and subsequently a different residence time. Production is reduced in the windy storm track regions of the Southern Hemisphere (due to the lower k_{PP} in this biologically productive region). By contrast, more CH_3I is produced in the warmer subtropical regions. The relative importance of outgassing is thus reduced compared to Opt1 (in the global budget; see Table 2), whereas the temperature- and light-dependent degradation processes gain in importance. The global oceanic residence time in this experiment is only 11 days (Table 2).

Photochemical production of CH_3I is parameterized as linearly coupled to the dissolved organic carbon (DOC) concentration and radiation. Experiment Opt3 uses the DOC pool of HAMOCC (Fig. 6b). This semi-labile DOC (SLDOC) originating from exudation by plankton is remineralized at a constant decay rate, and is transported by advection and diffusion. High DOC concentrations are thus located in highly productive regions (Fig. 6b), and dispersion within its lifetime of a few months leads to dilution of the gradients that originate from primary production (compare Figs. 4a and 6b). The spatio–temporal patterns of CH_3I follow the ones of SLDOC and roughly resemble the ones in Opt1, but at generally lower concentrations (Fig. 5). Global production is much lower in this experiment (approximately 125 Gg yr^{-1}, Table 2), but due to the similar spatial distribution of production, the residence time (approximately 17 days) is close to that of Opt1.

In a second experiment on photochemical production, the DOC concentration used in the CH_3I source parameterization was kept constant instead of using the prognostic DOC tracer. This mimics a "virtual" refractory DOC (RDOC) pool, i.e., an unlimited DOC supply. Here, the spatial distribution of CH_3I production is solely determined by incoming solar radiation (Fig. 6a). CH_3I concentrations are a function of the source strength relative to the sinks (degradation, outgassing), and hence the CH_3I concentration distribution does not directly reflect shortwave radiation, but rather differs significantly from it (Fig. 5). For example, in the tropical Pacific, the CH_3I concentration is strongly influenced by wind speed: in areas of higher wind speed, like the tropical easterlies north of the Equator (at 150° W westward), concentrations are lower than in areas of low wind speed closer to the American coast, due to enhanced outgassing. The residence time of 21 days is similar to the one in Opt1 and Opt3.

Two experiments were performed that considered more than one CH_3I production pathway: (1) Opt134, which includes "normal" biological production and photochemical production by degradation of refractory and semi-labile DOC, and (2) Opt24, which includes photochemical production by degradation of refractory DOC and biological production, including enhanced production during stress. In Opt134, the methyl iodide is almost exclusively produced via the photochemical production pathway; less than 1 % is produced by phytoplankton (Fig. 8, Table 2). 72 % are thereby

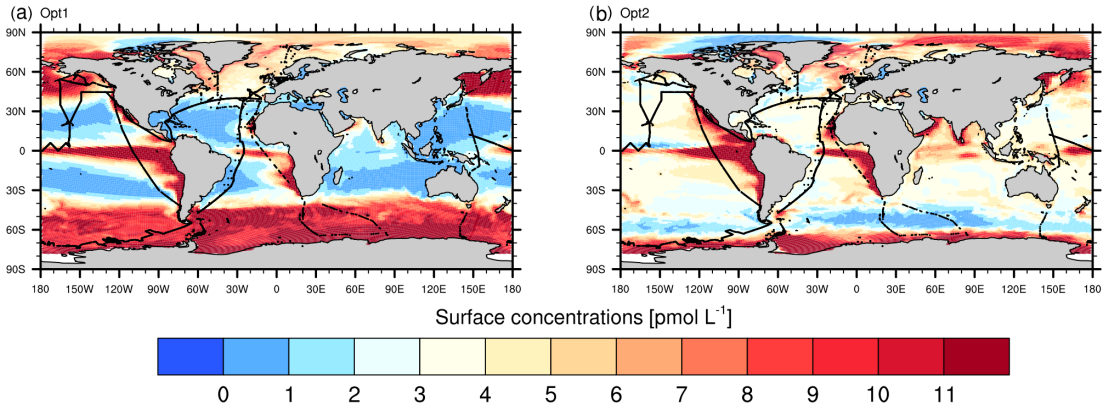

Figure 3. Annual mean methyl iodide concentration (pmol L^{-1}) in the experiment, with normal biological production, Opt1 **(a)**, and with production from stressed picocyanobacteria, Opt2 **(b)**. Black dots mark the sampling locations of CH_3I observations (shown in Fig. 1).

Table 3. Global fraction of observations best presented by the respective model experiment (as shown in Fig. 10 for individual locations and seasons), considering only single source experiments, only mixed source experiments, and all experiments (upper part). Global root mean square deviation (RMSD; pmol L^{-1}), root median square deviation (RMSD (median); pmol L^{-1}), and global median of the ratio $\frac{\text{observation}}{\text{model}}$ (lower part).

Source	Biological		Photochemical		Mixed	
ID	Opt1	Opt2	Opt3	Opt4	Opt134	Opt24
Percentage of simulated data closest to observations						
Including only single source exp.	13.12 %	24.15 %	16.46 %	46.27 %		
Including only mixed source exp.					39.31 %	60.69 %
Including all exp.	7.63 %	16.56 %	12.14 %	34.27 %	18.17 %	11.23 %
Characteristics of the comparison between model and observations						
Global RMSD (pmol L^{-1})	7.78	10.11	2.97	2.63	3.14	3.21
Global RMSD (median; pmol L^{-1})	1.04	0.65	0.50	0.35	0.60	0.52
Median ratio $\frac{\text{observation}}{\text{model}}$	2.14	1.74	3.42	2.01	1.24	1.49

produced via the unlimited DOC pool (RDOC), and 28 % from the semi-labile DOC (Table 2). The spatial distribution (Fig. 7) is very similar to the one in Opt4 (Fig. 5). Differences occur where production from SLDOC is strongest, i.e., in the equatorial Pacific, in the Southern Ocean in boreal winter and in the North Pacific in boreal summer. There, concentrations are higher than in Opt4, due to higher CH_3I production triggered by spatial DOC maxima (Fig. 6). The total CH_3I production in Opt134 is 60 % higher than in Opt4, but the inventory is only $\approx$ 10 % higher, as the additional production occurs in regions of high wind speed or temperature and outgases to the atmosphere (Fig. 12). The shift in the production towards warm and windy regions, which both support CH_3I loss, leads to a significant reduction in the global residence time in Opt134 (14 days) compared to Opt4 (21 days).

In Opt24, 70 % of the methyl iodide is produced via the photochemical, and 30 % via the biological production pathway (Table 2). Biological production dominates only in the equatorial Pacific and Atlantic, in the Southern Ocean in boreal fall (September–November), in the North Atlantic in spring, and in the Arctic in summer (boreal summer, not shown). Once more, this implies that production is enhanced in regions where the lifetime of CH_3I is low, as temperature and wind conditions favor degradation and outgassing. However, not all of the freshly produced CH_3I is lost, and the concentrations at, e.g., the Equator are enhanced compared to Opt4. The global production of 306 Gg yr^{-1} is in between the ones of the single source experiments, Opt2 (407 Gg yr^{-1}) and Opt4 (217 Gg yr^{-1}).

3.2 Comparison of simulated and observed CH_3I concentrations

The simulated surface methyl iodide concentrations are compared with observations (Figs. 1, 2, and 9; Figs. S1–S25 in the Supplement). Generally, the model represents methyl iodide observations well (Fig. 2 and Fig. S1–S25 in the Supplement), i.e., model-predicted surface concentrations are on

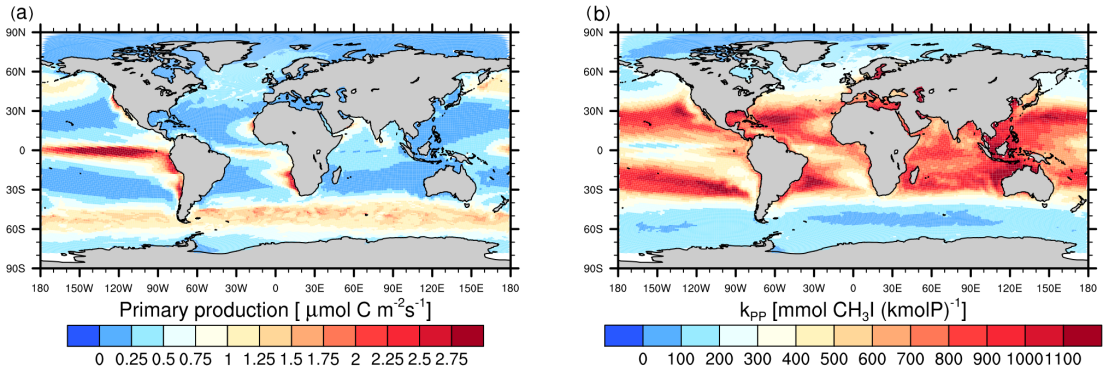

Figure 4. Integrated annual mean primary production ($\mu mol\, m^{-2}\, s^{-1}$) **(a)** and mean ratio between methyl iodide and primary production rate k_{PP} ($mmol\, CH_3I\, (kmolP)^{-1}$) **(b)**.

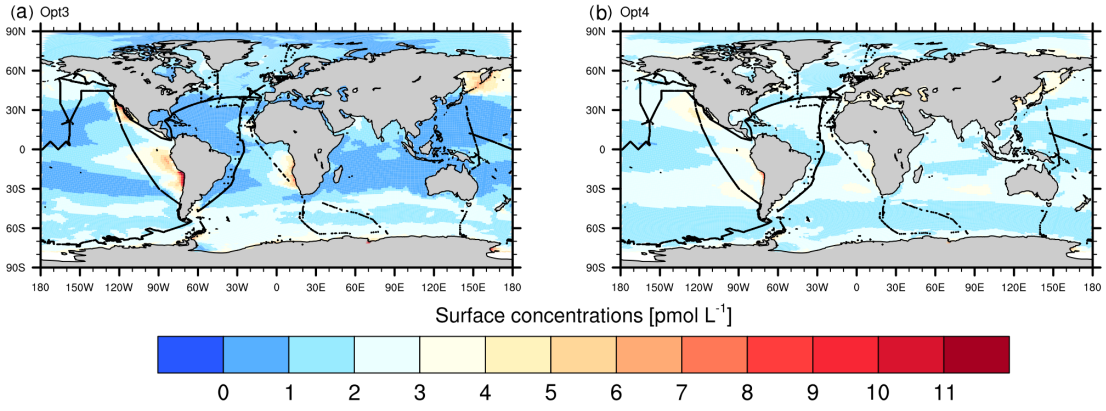

Figure 5. Annual mean methyl iodide concentration ($pmol\, L^{-1}$) in the experiment, with photochemical production from SLDOC, Opt3 **(a)**, and RDOC, Opt4 **(b)**. Black dots mark the sampling locations of the CH_3I observations (shown in Fig. 1).

the order of magnitude of the observed concentrations in all experiments. However, the quality of the simulated concentrations of the individual experiments varies between the regions (Fig. 2).

In the following, we look more closely at the magnitude, spatial gradients, and seasonal patterns of CH_3I concentrations in the Atlantic, the Pacific, and the Southern Ocean.

Observed concentrations in the Atlantic span a wide range, from $< 0.1\, pmol\, L^{-1}$ (Chuck et al., 2005) to $45\, pmol\, L^{-1}$ (Smythe-Wright et al., 2006), but values higher than $20\, pmol\, L^{-1}$ are rare in the open ocean, where typical concentrations are between $1\, pmol\, L^{-1}$ and $15\, pmol\, L^{-1}$ (Butler et al., 2007; Chuck et al., 2005; Jones et al., 2010; Schall et al., 1997; Wang et al., 2009) (see the Supplement for individual cruise data). In contrast to other biogenic organohalogens, methyl iodide concentrations often do not show a pronounced maximum at the Equator. Ship cruise data covering a broad range of latitudes in the Atlantic in boreal fall (cruise BLAST 2, October–November 1994 (Butler et al., 2007), Figs. 1 and 9a, Fig. S1 in the Supplement) reveal relatively homogeneous methyl iodide concentrations. Here, model experiments with biological CH_3I production (Opt1, Opt2) show an unrealistic maximum around the Equator, where nutrient upwelling, high temperatures, and high insolation favor phytoplankton growth. By including enhanced production by stressed picocyanobacteria, and not only "normal" biological production, the representation of CH_3I is significantly improved along the ship track in the Atlantic. In Opt1, CH_3I concentrations show steep gradients between low concentrations in the oligotrophic subtropical gyres and high concentrations in the nutrient-rich equatorial region. The consideration of a higher CH_3I production under nutrient shortage compensates for the low primary production, and brings CH_3I concentrations closer to observations. However, similarly to Opt1, this experiment (Opt2) overestimates observed concentrations at the Equator by a moderate factor of approximately 1.3.

Though the experiments that consider solely photochemical production do not show a strong latitudinal gradient along the ship track, they tend to underestimate observed methyl iodide concentrations. Observations are however also equivocal regarding that gradient: in contrast to Butler et al. (2007) (BLAST 2, Fig. S1 in the Supplement) and Chuck et al. (2005) (Polarstern cruise ANT XVII/1 in September

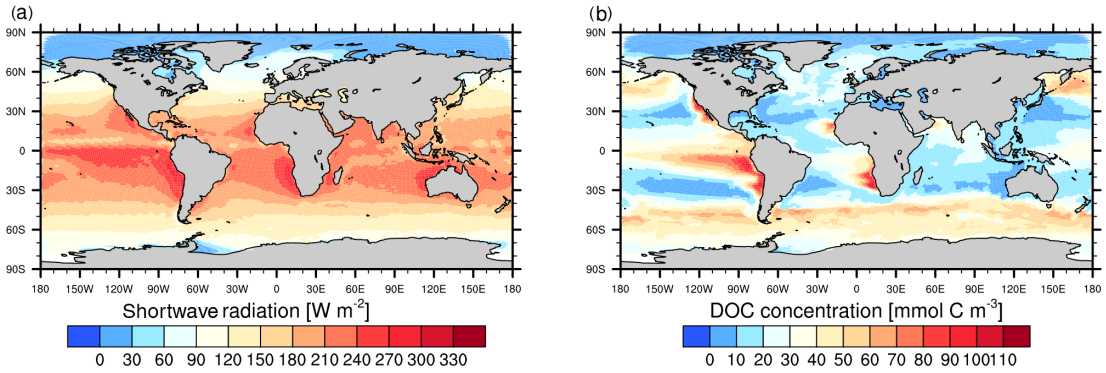

Figure 6. Annual mean shortwave radiation ($W\,m^{-2}$) **(a)** and semi-labile DOC concentration ($mm\,C\,m^{-3}$) **(b)**.

and October 2000, not shown), Tanzer and Heumann (1992) find an increase in CH_3I concentrations in the Atlantic towards the Equator on the same ship track (Polarstern cruise ANT VII/5 in March and April 1989, not shown).

Another feature is the east–west gradient in the subtropical North Atlantic in spring and summer (Fig. 9b, Fig. S10 in the Supplement) in the biological experiments. This gradient evolves from low production in oligotrophic areas and higher production in more nutrient-rich areas, and from subsequent DOC formation. Observations do not show this gradient, as concentrations in subtropical gyres are usually higher or equally as high as in other open ocean regions. This is improved in experiments Opt2 and Opt4, and in the mixed source experiments.

For the Atlantic, some information on the seasonal cycle of CH_3I concentrations is available from Wang et al. (2009). They find maxima in summer in the northeastern Atlantic south of Greenland (compare Figs. S21–S23 in the Supplement). The model experiments Opt1 and Opt2 show maxima in spring. Only those experiments in which photochemical production is dominant are able to reproduce the observed seasonality. They show maxima in summer with a similar magnitude and a similar difference between the seasons, as found in observations.

In Opt3, we use the parametrization of CH_3I production that was introduced in the work of Bell et al. (2002). In Bell et al. (2002), CH_3I concentrations have been overestimated in Labrador seawater by 1–2 orders of magnitude compared to Moore and Groszko (1999) and Moore and Tokarczyk (1993). In the experiment, Opt3 concentrations in Labrador seawater are reduced, but this does not imply a model improvement, as spatial gradients elsewhere (e.g., in subtropical gyres) are not represented satisfactorily (see above). In experiments Opt2 and Opt4, by contrast, concentrations in the Labrador Sea are improved compared to Bell et al. (2002), and spatial patterns in other ocean regions are similar to observed patterns. Both experiments show CH_3I concentrations of 2–7 $pmol\,L^{-1}$ in July and are in the range of observed concentrations in the Labrador Sea (1–6 $pmol\,L^{-1}$; Moore and Groszko, 1999). This is achieved without the implementation of an additional (biological) sink, which was suggested by Bell et al. (2002) to compensate for overestimations.

In the Pacific, observed concentrations range between 0.3 and 12 $pmol\,L^{-1}$ (Butler et al., 2007). There are fewer data for the western Pacific, and these reveal lower concentrations (often below 1 $pmol\,L^{-1}$) than in the eastern Pacific (3–12 $pmol\,L^{-1}$), though one has to note that the ship cruises are from different seasons. Model results also show lower values in boreal fall in the western Pacific, and higher values in the eastern Pacific. Experiments with the biological production of methyl iodide show partly strong CH_3I concentration overestimations of up to a factor of 5 in biologically productive areas, such as the tropical Pacific (Fig. 9c, d and Figs. S8, S11, S13 in the Supplement) or areas of coastal upwelling (Fig. S9 in the Supplement). Although HAMOCC is a state-of-the-art marine biogeochemical model, certain aspects have to be considered that affect methyl iodide production. Biological production of CH_3I in the model is proportional to primary production, which can not be evaluated easily on a global scale. The biogeochemical model is tuned to capture the main features of the nutrient (phosphate, nitrate, iron) distributions, and to simulate reasonably export production. Some features, like the large-scale distribution of primary production, are well represented, as primarily driven by nutrient supply and insolation. One known weakness, in more or less all global models, is the so-called "nutrient trapping" in the equatorial Pacific (summarized in Dietze and Loeptien, 2013), where excessively high nutrient concentrations at the surface lead to excessively high primary and export production in the equatorial Pacific. Differences between modeled and observed CH_3I concentrations in the tropical Pacific (e.g., Fig. 9c) hence can not be unambiguously translated into the likelihood of a certain production pathway.

In the Southern Ocean, observations show both concentrations lower than 5 $pmol\,L^{-1}$ (e.g., west of 66° W in spring (MAM); Fig. 1) and values higher than 5 $pmol\,L^{-1}$ (30–90° E in MAM). The distinct seasonal cycle seen in many

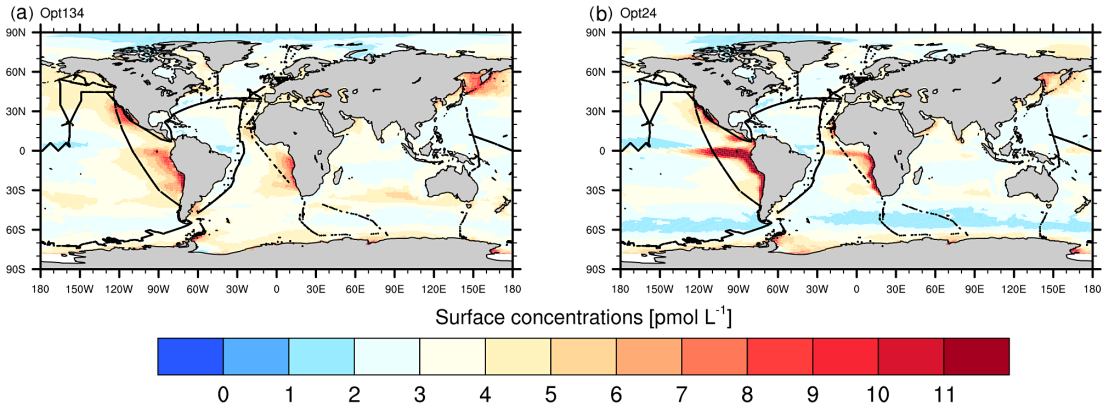

Figure 7. Methyl iodide concentration (pmol L^{-1}) in the experiment with mixed biological and photochemical production, Opt134 **(a)**, and the one with mixed biological production considering stressed picocyanobacteria and photochemical production from RDOC, Opt24 **(b)**. Black dots mark the sampling locations of the CH_3I observations (shown in Fig. 1).

model experiments can not be extracted from observations, because the data coverage is sparse. Also, a higher coverage might not show this feature clearly, because the concentration distribution is very variable in that region (see Figs. S14–S20 in the Supplement).

3.3 Identification of the dominating CH_3I source

After analyzing the differences between simulated and observed CH_3I concentrations, we now aim to determine the production pathway(s) that dominate(s) surface concentrations. To accomplish this for each location, the experiment was identified for which simulated concentrations match the observed values most closely. This was done first by calculating the absolute deviation between simulated and observed concentrations for each observational data point and experiment. After ranking the experiments, the experiments that show the lowest deviation are mapped (Fig. 10), and the number of occasions when the deviation of a particular experiment was lowest was counted. Table 3 lists these numbers for each experiment relative to the total number of observations. As this is only a relative measure, three additional indicators are derived: the global root mean of the individual squared deviations, the global root median of the individual squared deviations (as they are not symmetrically distributed, see SI Fig. S28), and the median of the individual ratios of observations and simulated concentrations (to account for the spatial variability of concentrations).

First we start with the hypothesis that CH_3I is produced via one dominating source process; thus we only consider Opt1 to Opt4 in the analysis. At first, none of the ship cruises or seasons shows a concordant preference for one single experiment, but instead they show a mixture of various sources best representing certain locations, without any obvious pattern (Fig. 10a). Testing if the deviation factor between modeled and observed concentrations is determined by some physical or biological mechanism did not reveal any systematic feature, e.g., higher/lower deviations in regions with high/low primary production. This means that the underestimations in oligotrophic regions are equally as high as, e.g., overestimations in productive regions. On a global scale, Opt4 (the experiment that mimics photochemical production from RDOC) is the most successful one among the single source experiments, showing the lowest deviation for 46.27 % of the observations, followed by Opt2, which represents 24.15 % of the observations best (Table 3). The differences of root mean and root median square deviations (Table 3) illustrate the pronounced skewness of the distribution of the squared deviations. Globally, the deviation of simulated and observed concentrations is lower for Opt4 compared to Opt1, Opt2, and Opt3. The second-lowest deviation globally is found for experiment Opt3, in contrast to the second rank in the number of best matches found for Opt2. This simply reflects the spatial inhomogeneity of the deviations: whereas Opt2 is closer to the observations more often than Opt3, the deviations are higher, in particular in the biologically productive equatorial upwelling. Opt3 furthermore underestimates observations more strongly than Opt4 and Opt2, indicated by the highest median ratio of observations and simulated concentrations. The robustness of these results is tested by performing a number of additional sensitivity experiments, in which input parameters and forcing data are changed.

A variation in the production ratios by 10 % in Opt1, Opt3, and Opt4 leads to the same spatial distribution (Figs. S26 and S27 in the Supplement), and the PDF (probability density function) of the ratio observation/model (Fig. S28 in the Supplement) is unchanged. This is also true when a different forcing (transient NCEP 6 h data (Behringer and Xue, 2004) instead of climatological daily mean OMIP) is used in Opt4 (e.g., Fig. S29 in the Supplement). Differences in the RMSD and the ranking (Table 3) of the experiments are thus robust and driven by the spatial distribution of the concentrations rather than by the choice of production rates. In particular,

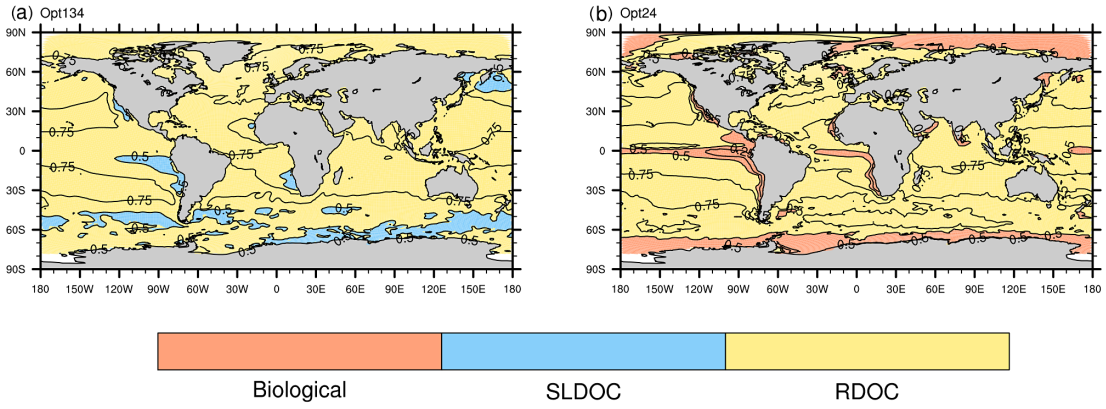

Figure 8. Source apportionment (shaded contours: local dominant source; black contour lines: fraction of photochemical production from RDOC) in the experiment with mixed biological and photochemical production, Opt134 **(a)**, and the one with mixed biological production considering stressed picocyanobacteria and photochemical production from RDOC, Opt24 **(b)**.

Opt1 and Opt3 are the least successful, because their spatial distribution is determined by primary production, which shows features that are not present in global patterns of observed methyl iodide. In contrast to model results, observations do not show low concentrations in oligotrophic subtropical gyres and high concentrations in productive regions. However, one has to keep in mind that halocarbon production rates are different for different phytoplankton species (Moore and Tokarczyk, 1993; Hughes et al., 2006; Smythe-Wright et al., 2006; Brownell et al., 2010); community composition differences would hence lead to changes in the bulk CH_3I production rate and distribution patterns. The inhomogeneity of the community composition and the CH_3I production rate implies that chlorophyll *a* may also not be a good predictor of CH_3I production (see also Sect. 3.2). The success of Opt4 over Opt3 shows that the representation of DOC does indeed strongly influence the ability of the model to reproduce observed concentrations when considering photochemical production alone. Where Opt3 shows minima due to low DOC, Opt4 shows maxima due to high insolation. These differences are higher than differences that arise from variable insolation (i.e., Opt4 with OMIP forcing compared to Opt4 with diurnal NCEP forcing in different years). In reality, biological and photochemical production most likely occur at the same time.

In the next step, we assume that methyl iodide is always produced from mixed biological and photochemical sources; thus we consider only Opt24 and Opt134 in the analysis. The number of "best matches" identifies Opt24 as the more successful experiment, being closest to approximately 60 % of the observations (Table 3). The comparison of root mean and root median squared deviations, and the median ratio of observed and simulated concentrations, show (Table 3) that both experiments represent observations equally well. This comes as no surprise, as photochemical production is the dominant source in both experiments (Fig. 8). This also explains why the mixed source experiments do not lead to significant improvements over the single source experiments. Of course, repeated parameter optimizations with different criteria, e.g., weighting of deviations in biologically productive or upwelling regions, may lead to a different source apportionment, and could result in different concentration distributions compared to the single source experiments. We refrain from conducting this, because it would not lead directly to new insights into the substances, but would rather constitute a fine-tuning of the model.

As a final step, we do not restrict the analysis to the number or nature of CH_3I source processes, but take all experiments into account. The analysis of the number of lowest deviations reveals that photochemical production from RDOC, i.e., Opt4, globally explains the large fraction of observations (34 %), followed by Opt134 (18 %) and Opt2 (16 %). This is also reflected by the fact that Opt4 shows the lowest overall (i.e., global mean and median) deviation from observations.

3.4 Covariation of CH_3I with biotic and abiotic variables

Covariation of proxy parameters (such as temperature, radiation, or chlorophyll concentration) with measured methyl iodide concentrations are often used to identify the dominant production pathway (e.g., Rasmussen et al., 1982; Happell and Wallace, 1996; Abrahamsson et al., 2004; Chuck et al., 2005; Wang et al., 2009; Lai et al., 2011). Formally this analysis is flawed, as none of the variables is truely statistically independent. However, in the current study, we know exactly which production process the simulated methyl iodide originates from, so we can test the robustness of some common predictors. For this purpose, the correlations between simulated methyl iodide surface concentrations and simulated temperature (sst), phytoplankton concentration (phy), as well as solar radiation (rad) along an arbitrary track (the 30° W meridian of 60° N–60° S), were derived for each

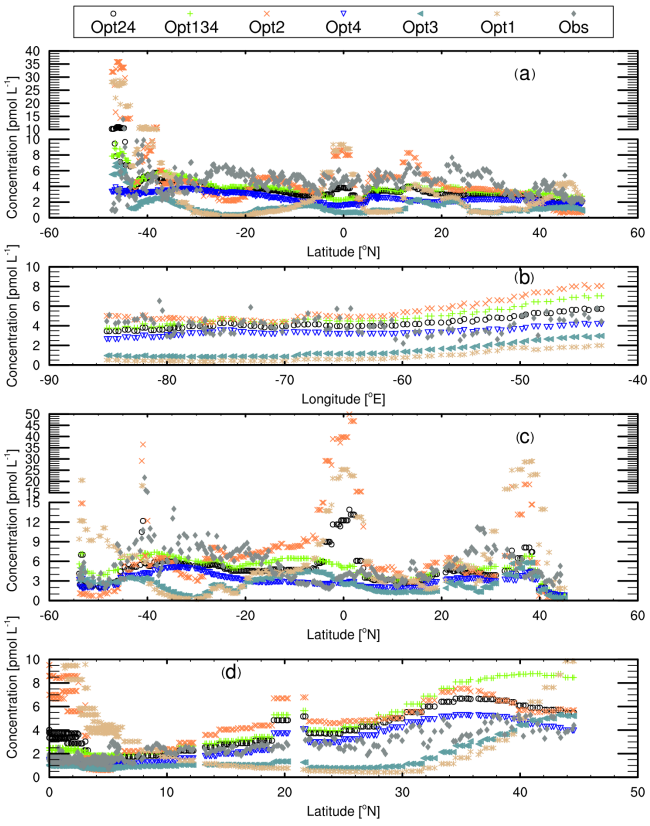

Figure 9. Observed and modeled methyl iodide concentrations (pmol L^{-1}). Observations are from Butler et al. (2007) (**a**: BLAST 2, **b**: Gas Ex 98, **c**: BLAST 1, **d**: Phase 1-04. See also Figs. S1, S8, S10, and S11 in the Supplement). Note the broken *y* axes in **(a)** and **(c)**.

month individually. For the CH_3I concentrations simulated in Opt1, the correlation with the phytoplankton concentration is always stronger than the ones with temperature or radiation (Fig. 11). For Opt2, by contrast, the correlation with radiation is strongest in some months, and no covariation with phytoplankton is observed (in September, $R(CH_3I,phy) < 0.1$ and $R(CH_3I,rad) = 0.79$). For Opt3, the covariation analysis along 30° W shows a strong relation to both phytoplankton and radiation in nearly all months (Fig. 11). The temporal pattern of correlation coefficients thereby follows the one of the correlation of the two parameters (R(phy,rad), Fig. 11d), and only when this correlation is low, e.g., in September and October, is the correlation with temperature highest. In Opt4, methyl iodide co-varies with radiation, and in all months CH_3I shows high, statistically significant, correlation coefficients (i.e., 0.6–0.9; Fig. 11). However, the correlations with phytoplankton and temperature are also high, and often (in January, February, October, and December) even higher than correlations with radiation.

From the source apportionment (Fig. 7), one expects for both experiments with mixed CH_3I sources similar correlation coefficients with temperature, phytoplankton and radiation as in Opt4, as photochemical production from a constant DOC pool is almost everywhere the dominant production pathway (apart from a small region around the Equator in Opt24, where biological production is equally important; see Fig. 7b). As a matter of fact, the temporal pattern of the correlation coefficients is almost identical between Opt4, Opt134, and Opt24. When looking into individual months, in Opt24, either the correlation with phytoplankton or the correlation with radiation is highest. Opt123 shows the same order in the correlation coefficients as Opt4, except in March.

3.5 Gas exchange with the atmosphere

Air–sea exchange is analyzed for Opt4, where observed CH_3I concentrations are represented best, and for Opt24 and Opt134, the experiments with mixed CH_3I sources.

As the prescribed atmospheric boundary conditions are identical in all experiments, differences between simulated saturation anomalies and gas fluxes are controlled only by differences in CH_3I dissolved in surface sea water. Air–sea fluxes can be both positive (into air) and negative (into the ocean), depending on the season and location (Fig. 12). The seasonal mean emission ranges from −200 to 1500 pmol m^{-2} h^{-1}. In line with the highest concentrations, the strongest outgassing is simulated in boreal winter in the Southern Ocean, where high production co-locates with high wind speeds. Note that the seasonal mean distributions shown in Fig. 12 suggest a strong spatial homogeneity, which in reality does not exist. At higher temporal resolutions (e.g., daily means), the emissions are very "patchy", and the flux in neighboring regions in the Southern Ocean can differ by more than 1000 pmol m^{-2} h^{-1} (see Fig. S30 in the Supplement, daily mean emissions over the first 120 days of the year). This inhomogeneity is caused by small-scale low-pressure systems that travel along the Southern Hemisphere storm track and lead to episodic high wind speeds. Furthermore, the daily mean data are characterized by a wider range of fluxes (−225 to 3687 pmol m^{-2} h^{-1}) than the seasonal means (see above).

In boreal summer, strong outgassing is found in the mid-latitude North Atlantic and North Pacific. Generally, lower emissions are predicted for the tropical and polar regions. This is due to weaker winds that partly lead to low emissions, despite high production (e.g., in Opt24 in the tropical Pacific). In polar regions, the sea ice cover seasonally shields the ocean from direct contact with the atmosphere, and thereby suppresses outgassing. In all experiments, a reversal of the air–sea flux is predicted for the same region in boreal winter in the North Atlantic (> 50 °N).

Overall, global annual fluxes range from 100 to 170 Gg yr^{-1} (Table 2), with the ocean acting as a net source of methyl iodide for the atmosphere. Global emissions reported in the literature are often estimated from observed oceanic concentrations (and, ideally, simultaneously measured atmospheric concentrations), which are used first to

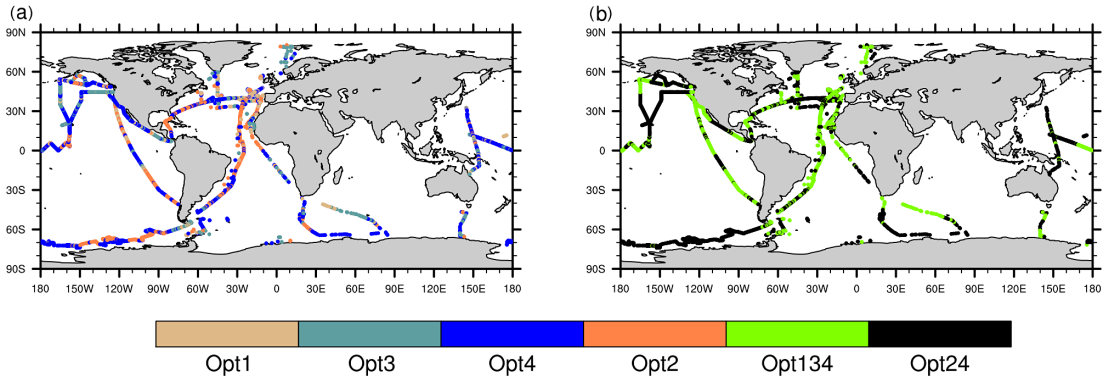

Figure 10. Experiment closest to the observed concentration at the sea surface, when considering only single source experiments **(a)**, and only mixed source experiments **(b)**.

Table 4. Global annual methyl iodide emissions ($Gg\,yr^{-1}$) from the ocean.

Source type	Lit. value	This study	Reference
Open ocean		101.52–170.6	Opt4, Opt134
Open ocean	270		Liss and Slater (1974)
"Unproductive" ocean	50		Rasmussen et al. (1982)
"Moderately productive" ocean	220		Rasmussen et al. (1982)
"Highly productive" ocean	1000		Rasmussen et al. (1982)
Open ocean	300–500		Singh et al. (1983)
Global ocean	150		Campos et al. (1996)
Global ocean	130–350		Moore and Groszko (1999)
Open ocean	214		Bell et al. (2002)
Open ocean, 40° N–40° S	610	174 (219*)	Smythe-Wright et al. (2006), Opt2
Open ocean	298.1		Butler et al. (2007)
Global ocean	610.4		Butler et al. (2007)
Oligotrophic open ocean	138.6		Jones et al. (2010)
Mesotrophic open ocean	133.5		Jones et al. (2010)
Global ocean	205.8		Ziska et al. (2013) (OLS)
Global ocean	176.0		Ziska et al. (2013) (RF)

* Global value.

calculate an emission flux, which is then extrapolated to the global scale (e.g., Liss and Slater, 1974; Moore and Groszko, 1999; Smythe-Wright et al., 2006; Butler et al., 2007; Ziska et al., 2013). Global emissions simulated here are at the lower end of these previously estimated values (Table 4). In general, deviations can be due to both, emissions estimated from observations and the simulated fluxes, so all values listed in the table are discussed separately.

The global flux of $270\,Gg\,yr^{-1}$ reported in Liss and Slater (1974) is calculated from observations of CH_3I in the marine boundary layer of the Atlantic (approximately 60° N–50° S) collected during a ship cruise in 1970–1971 (Lovelock et al., 1973). Unfortunately, only the mean values of atmospheric and oceanic volume mixing ratios are reported, together with the note that they did not find any obvious latitudinal trend, but large local variations. Our results also suggest only a weak latitudinal variation in the seawater concentration in fall (Fig. 1) across the Atlantic (Opt4, Opt134, and Opt24), but a strong seasonal variation, with concentrations lower ($< 0.5\,pmol\,L^{-1}$) than the value reported in Lovelock et al. (1973). In particular, our simulations suggest a reversal of the flux in the North Atlantic in winter. Altogether, this can lead to deviations in the simulated global flux, which is approximately 35–50 % lower.

Rasmussen et al. (1982) aggregate more than 450 samples of atmospheric concentrations and only 21 samples of oceanic concentrations (which were not taken simultaneously) into fluxes for biologically unproductive, moderately productive, and highly productive regions. These are assumed to hold a share of 60, 30, and 10 % of the ocean surface, respectively. For the comparison, we omit the contribution of the highly productive coastal regions, because of the coarse spatial resolution of the global model. The emissions estimate is identical to the one by Liss and Slater (1974), and

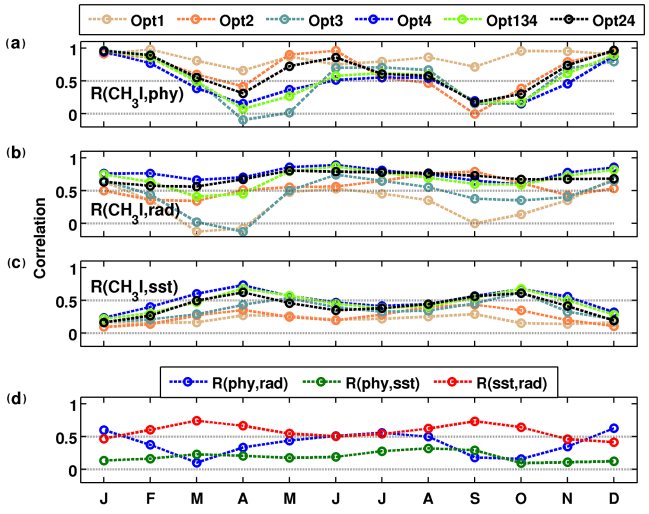

Figure 11. Spatial correlation of the monthly methyl iodide surface concentrations along the 30° W meridian (60° N–60° S), with surface phytoplankton concentrations **(a)**, radiation **(b)** and sea surface temperature **(c)**, and spatial correlations of phytoplankton and radiation (R(phy,rad)), phytoplankton and SST (R(phy,sst)), and SST and radiation (R(sst,rad)) **(d)**. All correlations are significant on the 95 % level.

the deviation arises from the same causes, namely an underrepresentation of the seasonal variation in seawater concentrations and the simulated temporal reversal of gas exchange.

Singh et al. (1983) measured CH_3I in seawater and air on a ship cruise in November–December 1981 in the eastern Pacific, close to the American coast. The measured mean air concentration of 2 ppt is higher than the atmospheric concentrations used for modeling in that region (0.5–1.5 ppt, see Ziska et al., 2013). Simulated oceanic concentrations across that ship track range from 2.5 to 3.9 pmol L^{-1} in Opt4, and from 3 to 35 pmol L^{-1} in Opt24 and Opt134, and are comparable with the observed range of approximately 3–47 pmol L^{-1}. Hence, our simulated fluxes may be slightly higher here, despite comparable seawater concentrations, due to a stronger saturation anomaly. Since the simulated concentrations (and fluxes) along the ship track are higher than in other oceanic regions (see Fig. 10a, e, i and d, h, l), the global flux is subsequently lower than the estimate by Singh et al. (1983).

Campos et al. (1996) measured CH_3I in the North Sea and reported sea water concentrations of 3–14 pmol L^{-1}. They estimated an average annual flux of 374.8 pmol m^{-2} h^{-1}. This value is close to those simulated in the North Sea (though the model is not meant to reproduce conditions there), and at the same time close to the global mean value of simulated annual mean emissions (e.g., 385 pmol m^{-2} h^{-1} in Opt134). It is only by chance that extrapolating the value found in the North Sea to a global CH_3I flux, assuming a globally homogeneous distribution, leads to a value similar to the simulated one, as the assumption is invalid.

The emissions estimate presented by Moore and Groszko (1999) is based upon concentrations in air and water derived from three ship cruises in the Labrador and Sargasso seas (July 1995), the Pacific from 47° N on the US coast to 47° S in Australia (Seattle–Hobart in October–November 1995), and the eastern Atlantic off Ireland (June 1996). Based on these measurements, they calculated a CH_3I flux of 666.7 (75–2666.7) pmol m^{-2} h^{-1} for the Pacific, 495.8 (12.5–2292) pmol m^{-2} h^{-1} for the Labrador Sea, and 1041 (12.5–4500) pmol m^{-2} h^{-1} for the eastern Atlantic. Using these values, and an uncertainty analysis of the wind speed data, they came up with a global range of approximately 130–350 Gg yr^{-1}. The derived local fluxes are in line with our simulated values, and deviations between the global values are again caused by spatial and temporal variations.

Bell et al. (2002) calculated their emissions from a model simulation that uses the same parameterization of CH_3I production as in Opt3. As our simulated seawater concentrations at many locations are lower than those simulated by Bell et al. (2002), our global CH_3I flux is consequently lower, despite similar air concentrations. Notably, their model simulation does not predict a reversal of the gas exchange in the northern Atlantic. Here our model predicts a seasonal mean of 0.2–0.3 ng L^{-1} in seawater, which is lower than the value in Bell et al. (2002) (0.5 ng L^{-1}); atmospheric concentrations in that particular region are approximately 0.9 ppt (0.6–0.97 ppt), which is slightly higher than their value of 0.6 ppt.

Smythe-Wright et al. (2006) report a mean CH_3I flux produced by *Prochlorococcus* from their ship cruise measurements of oceanic and atmospheric concentrations of 109.5 nmol m^{-1} d^{-1}. Based on this value and the ocean surface in the area of *Prochlorococcus* occurrence (at lower latitudes; 40° S–40° N), they estimate a contribution of 610 Gg yr^{-1}. This result can best be compared to the values simulated in Opt2, the experiment that mimics *Prochlorococcus*, and enhanced production during stress, in which temporally, i.e., during strong nutrient limitation, the production ratio k_{PP} is close to the one suggested in Smythe-Wright et al. (2006) (see Fig. 4b and Stemmler et al., 2013). Our experiment Opt2 shows that the biological contribution is much lower, i.e., 173 Gg yr^{-1}. Two aspects explain the difference. First, the maximum concentration in Opt2 is lower than the observed maximum of 40 pmol L^{-1}. Second, Smythe-Wright et al. (2006) assume that these high concentrations prevail all year long, whereas the model simulation resolves an intra-annual variation. Since in Opt2 the majority of the flux is within the region 40° N–40° S, the global emissions are only marginally higher (218.6 Gg yr^{-1}, Table 2).

The global emissions estimates by Butler et al. (2007) are based on observed CH_3I from seven ship cruises from 1994 to 2004, covering all seasons. They cluster the results into fluxes of four types: “Tropics”, “Southern Ocean”, “Gyres”, and “Coastal waters”. The measured atmospheric concentrations are consistent with the ones used in this study.

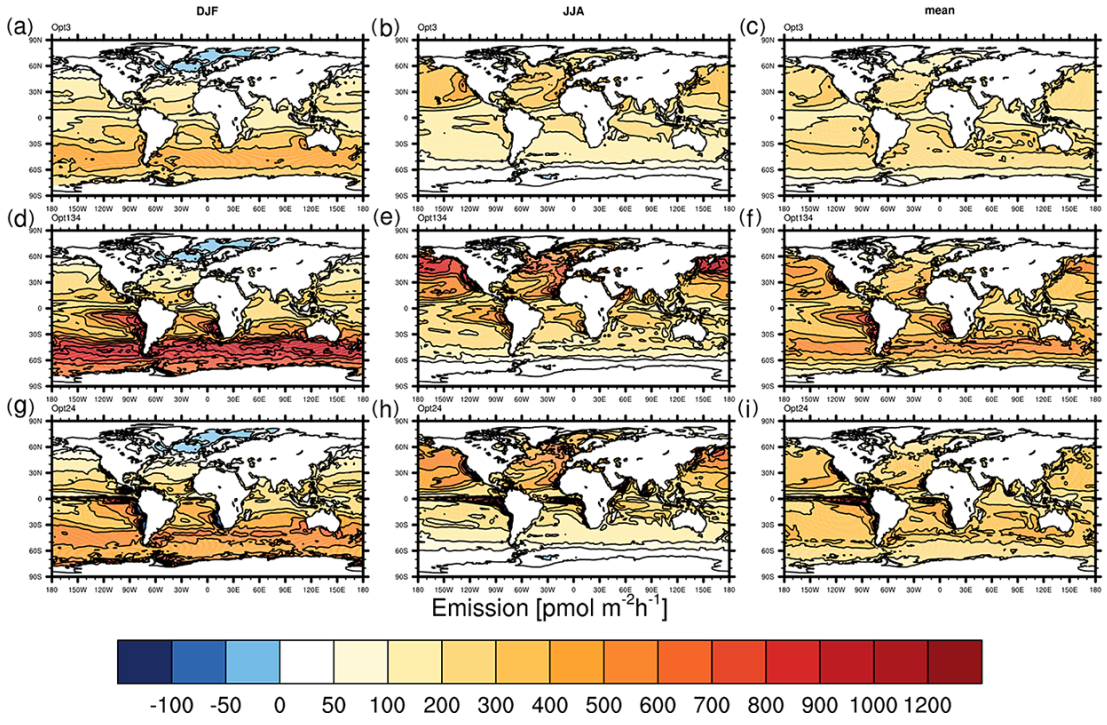

Figure 12. Emissions into the atmosphere (pmol m^{-2} h^{-1}) in Opt4 **(a–c)**, Opt134 **(d–f)** and Opt24 **(g–i)** in DJF **(a, e, i)** and in JJA **(c, g, k)**; annual mean **(c, f, i)**.

They calculate mean fluxes of 542 pmol m^{-2} h^{-1} for the "Tropics", 708 pmol m^{-2} h^{-1} for the "Southern Ocean", and 583 pmol m^{-2} h^{-1} for the "Gyres". These values are comparable to the simulated fluxes, though the regional distribution (i.e., the ratio between the defined clusters) is different for different experiments, and shows a clear seasonality. Also, their global estimate here for the open ocean is lower than our simulated value, due to the seasonal and spatial variability. In detail, e.g., their value for the Southern Ocean is determined from ship cruises in November–December 2001 and February–April 1996. Our simulation suggests that concentrations and fluxes are higher in these months than in austral winter. They furthermore do not cover the winter season in the region, where the model predicts subsaturation of the ocean by CH_3I. It is thus consistent that our simulated global values are lower than the estimates in Butler et al. (2007).

Jones et al. (2010) estimate regional emissions from the oligotrophic and mesotrophic open ocean, shelf, coastal, and upwelling regions from simultaneous measurements of seawater and air concentrations during two ship cruises in the North Atlantic in June–July 2006 (shelf, coastal, and upwelling are not listed in Table 4). Their mean seawater concentrations in the oligotrophic ocean are 6 pmol L^{-1}, whereas the model predicts approximately 3 pmol L^{-1}. In the open ocean between 15 and 25 °N, they find on average 16 pmol L^{-1}, while our model predicts 1–4 pmol L^{-1}. Also, concentrations in the open Atlantic (53–58 °N) are often higher in the observations (10.5, 3–21 pmol L^{-1}) than predicted values (6–9 pmol L^{-1}). The simulated values are in the range of observations, despite being at the lower end. Simulated fluxes are thus lower than those derived by Jones et al. (2010).

As the emissions calculated in Ziska et al. (2013) are based on observed atmospheric and oceanic CH_3I concentrations, and our simulations predict concentrations that are close to the observed values, and use observed atmospheric concentrations as the upper boundary conditions, the global emissions are similar (Table 4). Differences occur in particular where gaps in the observations were filled by an interpolation method. For instance, in the central to western Pacific Ocean (approximately 10–40° S, 90–180° W), where no observational seawater concentrations were available, a local maximum is predicted, which is not reflected in our model; by contrast, a local minimum is simulated here. Also, in the Indian Ocean, the emissions calculated by Ziska et al. (2013) rely solely on the extrapolation method. Here, their climatological flux is characterized by a distinct north–south gradient, with high values in the south. Though the gradient in their estimate by construction arises from remote observations, it is supported by the model simulations that also often predict a similar north–south gradient. In the climatology by Ziska et al. (2013), polar regions and the tropics are mostly in equilibrium; this is also the case in Opt4. Another prominent feature of their flux distribution pattern is the difference between the eastern and western Pacific at the lower latitudes (approximately 35° S–35° N), characterized by high values

in the east and low values in the west. This is also partly seen in the model results, e.g., in boreal winter in Opt134, despite differences in the exact location of maxima in the eastern Pacific (see above).

One feature that is simulated but not considered in most global estimates (apart from Ziska et al., 2013) is the reversal of the gas exchange. It is unclear whether the ocean can act as a sink for methyl iodide in certain locations and seasons. As the model uses temporally constant atmospheric boundary conditions based on observations with gaps filled by interpolation (Ziska et al., 2013), and as these observations in that region are particularly sparse, the robustness of the feature is uncertain. However, negative saturation anomalies in cold low-light waters in the Greenland and Norwegian seas were reported by Happell and Wallace (1996). They measured a mean atmospheric concentration of 2.4 pmol mol^{-1}, which is more than double the value we use in our simulations. We therefore believe that the reversal is indeed a feature of low production, rather than caused by overestimated air concentrations.

To sum up, simulated fluxes are consistent with fluxes calculated from observed concentrations in the marine boundary layer. Deviations from our calculated global emission and the estimates derived from extrapolating local fluxes to the global scale are minor, considering the spatial and temporal variability of the fluxes.

4 Conclusions

In this study, we show simulated global distribution patterns of CH_3I and air–sea fluxes. Different production pathways of CH_3I, i.e., biological and photochemical production mechanisms, are considered. This is the first study since Bell et al. (2002) that assesses marine emissions of CH_3I based on process parameterizations of its sources and sinks in the open ocean. The evaluation of all model experiments with an available global observational data set (Ziska et al., 2013) reveals that best agreement on the global scale is achieved when photochemicals from refractory DOC or both photochemical and direct biological production are considered. Specifically, the photochemical degradation of refractory detritus contributes to 70 % of CH_3I production; biological production by picocyanobacteria, including enhanced production during stress, accounts for the remaining 30 %. This pathway has been proposed by Hughes et al. (2011) based on laboratory experiments.

Our findings shed some light on the source mechanisms of CH_3I. Previous model studies (Bell et al., 2002) and field observations (e.g., Happell and Wallace, 1996; Chuck et al., 2005; Smythe-Wright et al., 2006; Wang et al., 2009) have suggested either a photochemical or biological source of CH_3I. In a recent model study, Stemmler et al. (2013) have shown that the observed vertical CH_3I profile in the tropical eastern Atlantic can be best explained by biological production. The model results obtained do not contradict all these previous findings. Including the photochemical pathway alone reflects the global observed distribution patterns reasonably well, if the availability of DOC is not limiting the process. Depending on the region or season, however, photochemical or biological production may dominate. For instance, in the Southern Ocean, the model suggests that biological production is dominant only in austral spring, while in the equatorial Pacific, CH_3I is biologically produced all year round. It is thus not surprising that correlations between methyl iodide and biotic or abiotic factors are not robust indicators for determining the source of CH_3I. The experiment where, e.g., only the photochemical pathway is considered, gives an equally high correlation coefficient of CH_3I with irradiance and phytoplankton, and in certain months with low irradiance, the correlation coefficient is even higher with phytoplankton. This is in line with Abrahamsson et al. (2004); based on observations, they conclude that chlorophyll *a* is not an adequate proxy for the production of organic halogens.

Despite the generally good agreement between model and observations, there are still some uncertainties that are related to regions where data are sparse (e.g., the Indian Ocean), or where seasonal variability is strong and the temporal resolution of observational data is insufficient (e.g., in the Southern Ocean). This is particularly crucial if the goal is to quantify emissions of methyl iodide. Our model results show that, globally, a net flux of methyl iodide from the ocean into the atmosphere takes place; however, on the local scale, the ocean can act both as a source and a sink of methyl iodide to the atmosphere. A flux from the atmosphere into the ocean takes place during the winter months at high latitudes of the North Atlantic Ocean. This seems to be a robust feature, because all model experiments show a net uptake of CH_3I by the ocean, regardless of the production pathway. So far there have been no observations that support or contradict this finding. We thus strongly suggest performing measurements in this region to test the performance of the model. A weakness of our current approach is the assumption of constant atmospheric concentrations that are used for the upper boundary condition. At least at high latitudes, strong seasonal variability can be expected. Using a coupled ocean–atmosphere model would account for this temporal variability.

Overall, we find significant differences in the emissions between the different model experiments. The production pathway is thus important for quantifying the air–sea fluxes. Global methyl iodide concentration can be reasonably well represented using time-averaged surface shortwave radiation. On a regional scale or at specific times, however, other source mechanisms can become dominant.

The Supplement related to this article is available online at doi:10.5194/bg-11-4459-2014-supplement.

Acknowledgements. The authors are grateful to F. Ziska (Geomar, Helmholtz Centre for Ocean Research, Kiel) for providing observational data, and for valuable discussions. We thank K. Six (Max Planck Institute for Meteorology, Hamburg) for an internal review of the manuscript, and the two anonymous referees for an external review of it. We thank C. Nam (University of Leipzig) for proofreading the manuscript. Model simulations have been performed with the IBM Power 6 supercomputer at the DKRZ (German Climate Computing Center). The study was funded by German BMBF project SOPRAN (Surface Ocean Processes in the Anthropocene), SOPRAN 03F0662E. I. Hense has been financed through Cluster of Excellence "CliSAP" (EXC177), University of Hamburg, funded by the German Science Foundation (DFG).

Our colleague E. Maier-Reimer died during the finalization of this manuscript. He annotated an earlier version, but had no chance to comment on the latest one. We hope that he would approve of the changes we made.

Edited by: L. Bopp

References

Abrahamsson, K., Bertilsson, S., Chierici, S., Fransson, A., Froneman, P., Lorén, A., and Pakhomov, E.: Variations of biochemical parameters along a transect in the Southern Ocean, with special emphasis on volatile halogenated organic compounds, Deep-Sea Res. Pt. II, 51, 2745–2756, 2004.

Amachi, S.: Microbial contribution to global iodine cycling: Volatilization, accumulation, reduction, oxidation, and sorption of iodine, Microbes Environ., 23, 269–276, 2008.

Amachi, S., Kamagata, Y., Kanagawa, T., and Muramatsu, Y.: Bacteria mediate methylation of iodine in marine and terrestrial environments, Appl. Environ. Microbiol., 67, 2718–2722, 2001.

Archer, S., Goldson, L., Liddicoat, M., Cummings, D., and Nightingale, P.: Marked seasonality in the concentrations and sea-to-air flux of volatile iodocarbon compounds in the western English Channel, J. Geophys. Res.-Oceans, 112, C08009, doi:10.1029/2006JC003963, 2007.

Behringer, D. and Xue: Evaluation of the global ocean data assimilation system at NCEP: The Pacific Ocean, in: Eighth Symposium on Integrated Observing and Assimilation Systems for Atmosphere, Oceans, and Land Surface, available online: https://ams.confex.com/ams/84Annual/techprogram/paper_70720.htm (last access: 15 August 2014), 2004.

Bell, N., Hsu, L., Jacob, D., Schultz, M., Blake, D., Butler, J., King, D., Lobert, J., and Maier-Reimer, E.: Methyl iodide: Atmospheric budget and use as a tracer of marine convection in global models, J. Geophys. Res., 107, 4340, doi:10.1029/2001JD001151, 2002.

Brownell, D., Moore, R., and Cullen, J.: Production of methyl halides by *Prochlorococcus* and *Synechococcus*, Global Biogeochem. Cy., 24, GB2002, doi:10.1029/2009GB003671, 2010.

Butler, J., King, D., Lobert, J., Montzka, S., Yvon-Lewis, S., Hall, B., Warwick, N., Mondell, D., Aydin, M., and Elkins, J.: Oceanic distributions and emissions of short-lived halocarbons, Glob. Biogeochem. Cy., 21, GB1023, doi:10.1029/2009GB003671, 2007.

Campos, M., Nightingale, P., and Jickells, T.: A comparison of methyl iodide emissions from sea water and wet depositional fluxes of iodine over the southern North Sea, Tellus B, 48, 106–114, 1996.

Carpenter, L.: Iodine in the Marine Boundary Layer, Chem. Rev., 103, 4953–4962, 2003.

Carpenter, L., Malin, G., Liss, P., and Küpper, F.: Novel biogenic iodine-containing trihalomethanes and other short-lived halocarbons in the coastal East Atlantic, Glob. Biogeochem. Cy., 14, 1191–1204, 2000.

Chameides, W. and Davis, D.: Iodine: Its Possible Role in Tropospheric Photochemistry, J. Geophys. Res., 85, 7383–7398, 1980.

Chuck, A., Turner, S., and Liss, P.: Oceanic distributions and air-sea fluxes of biogenic halocarbons in the open ocean, J. Geophys. Res.-Oceans, 110, 1–12, 2005.

Dietze, H. and Loeptien, U.: Revisiting "nutrient trapping" in global coupled biogeochemical ocean circulation models, Glob. Biogeochem. Cy., 27, 265–284, doi:10.1002/gbc.20029, 2013.

Elliot, S. and Rowland, F.: Methyl halide hydrolysis rates in natural waters, J. Atmos. Chem., 20, 229–236, 1995.

Elliott, S. and Rowland, F.: Nucleophilic substitution rates and solubilities for methyl halides in seawater, Geophys. Res. Lett., 20, 1043–1046, 1993.

Fuhlbrügge, S., Krüger, K., Quack, B., Atlas, E., Hepach, H., and Ziska, F.: Impact of the marine atmospheric boundary layer conditions on VSLS abundances in the eastern tropical and subtropical North Atlantic Ocean, Atmos. Chem. Phys., 13, 6345–6357, doi:10.5194/acp-13-6345-2013, 2013.

Fuse, H., Inoue, H., Murakami, K., Takimura, O., and Yamaoka, Y.: Production of free and organic iodine by *Roseovarius* spp., FEMS Microbiol. Lett., 229, 189–194, 2003.

Gibson, J., Kallberg, P., Uppala, S., Hernandez, A., Nomura, A., and Serrano, E.: ECMWF Re-Analysis, Project Report Series, l. ERA Description, Tech. rep., European Centre for Medium-Range Weather Forecasts, Reading, England, 1997.

Giese, B., Laturnus, F., Adams, F. C., and Wiencke, C.: Release of volatile iodinated C_1-C_4 hydrocarbons by marine macroalgae from various climate zones, Environ. Sci. Technol., 33, 2432–2439, doi:10.1021/es980731n, 1999.

Gschwend, P., MacFarlane, J., and Newman, K.: Volatile halogenated organic compounds released to seawater from temperate marine macroalgae, Science, 227, 1033–1035, 1985.

Happell, J. and Wallace, D.: Methyl iodide in the Greenland/Norwegian Seas and the tropical Atlantic Ocean: Evidence for photochemical production, Geophys. Res. Lett., 23, 2105–2108, 1996.

Hughes, C., Malin, G., Nightingale, P., and Lisa, P.: The effect of light stress on the release of volatile iodocarbons by three species of marine microalgae, Limnol. Oceanogr., 51, 2849–2854, 2006.

Hughes, C., Malin, G., Turley, C., Keely, B., Nightingale, P., and Liss, P.: The production of volatile iodocarbons by biogenic marine aggregates, Limnol. Oceanogr., 53, 867–872, 2008.

Hughes, C., Franklin, D., and Malin, G.: Iodomethane production by two important marine cyanobacteria: *Prochlorococcus marinus* (CCMP 2389) and *Synechococcus* sp. (CCMP 2370), Mar. Chem., 125, 19–25, 2011.

Ilyina, T., Six, K. D., Segschneider, J., Maier-Reimer, E., Li, H., and Núñez Riboni, I.: Global ocean biogeochemistry model HAMOCC: Model architecture and performance as component of the MPI-Earth system model in different CMIP5 experimental realizations, J. Adv. Model. Earth Syst., 5, 287–315, doi:10.1029/2012MS000178, 2013.

Itoh, N., Tsujita, M., Ando, T., Hisatomi, G., and Higashi, T.: Formation and emission of monohalomethanes from marine algae, Phytochemistry, 45, 67–73, 1997.

Jones, C., Hornsby, K., Sommariva, R., Dunk, R., Von Glasow, R., McFiggans, G., and Carpenter, L.: Quantifying the contribution of marine organic gases to atmospheric iodine, Geophys. Res. Lett., 37, L18804, doi:10.1029/2010GL043990, 2010.

Karlsson, A., Auer, N., Schulz-Bull, D., and Abrahamsson, K.: Cyanobacterial blooms in the Baltic – A source of halocarbons, Mar. Chem., 110, 129–139, 2008.

Lai, S., Williams, J., Arnold, S., Atlas, E., Gebhardt, S., and Hoffmann, T.: Iodine containing species in the remote marine boundary layer: A link to oceanic phytoplankton, Geophys. Res. Lett., 38, L20801, doi:10.1029/2011GL049035, 2011.

Liss, P. and Slater, P.: Fluss of gas aceross the air-sea interface, Nature, 247, 181–184, 1974.

Lovelock, J., Maggs, R., and Wade, R.: Halogenated hydrocarbons in and over the Atlantic, Nature, 241, 194–196, 1973.

Manley, S.: The possible involvement of methylcobalamin in the production of methyl iodide in the marine environment, Mar. Chem., 46, 361–369, 1994.

Manley, S. and Dastoor, M.: Methyl iodide (CH_3I) production by kelp and associated microbes, Mar. Biol., 98, 477–482, 1988.

Manley, S. and De La Cuesta, J.: Methyl iodide production from marine phytoplankton cultures, Limnol. Oceanogr., 42, 142–147, 1997.

Marsland, S., Haak, H., Jungclaus, J., Latif, M., and Röske, F.: The Max-Planck-Institute global ocean/sea ice model with orthogonal curvilinear coordinates, Ocean Model., 5, 91–127, 2003.

Moore, R. and Groszko, W.: Methyl iodide distribution in the ocean and fluxes to the atmosphere, J. Geophys. Res.-Oceans, 104, 11163–11171, doi:10.1029/1998JC900073, 1999.

Moore, R. and Tokarczyk, R.: Volatile biogenic halocarbons in the northwest Atlantic, Glob. Biogeochem. Cy., 7, 195–210, 1993.

Moore, R. and Zafiriou, O.: Photochemical production of methyl iodide in seawater, J. Geophys. Res., 99, 16415–16420, 1994.

Nightingale, P., Malin, G., and Liss, P.: Production of chloroform and other low-molecular-weight halocarbons by some species of macroalgae, Limnol. Oceanogr., 40, 680–689, 1995.

Nightingale, P. D., Malin, G., Law, C., Watson, A., Liss, P., Liddicoat, M., Boutin, J., and Upstill-Goddard, R.: In situ evaluation of airsea gas exchange parameterizations using novel conservative and volatile tracers, Global Biogeochem. Cy., 14, 373–387, 2000.

Orlikowska, A. and Schulz-Bull, D.: Seasonal variations of volatile organic compounds in the coastal Baltic Sea, Environ. Chem., 6, 495–507, 2009.

Rasmussen, R., Khalil, M., Gunawardena, R., and Hoyt, S.: Atmospheric methyl iodide (CH_3I) (Oregon)., J. Geophys. Res., 87, 3086–3090, 1982.

Rattigan, O., Shallcross, D., and Cox, R.: UV absorption cross-sections and atmospheric photolysis rates of CF_3I, CH_3I, C_2H_5I and CH_2ICl, J. Chem. Soc. Faraday T., 93, 2839–2846, 1997.

Richter, U. and Wallace, D.: Production of methyl iodide in the tropical Atlantic Ocean, Geophys. Res. Lett., 31, 1–4, 2004.

Röske, F.: A global heat and freshwater forcing dataset for ocean models, Ocean Model., 11, 235–297, 2006.

Schall, C., Heumann, K., and Kirst, G.: Biogenic volatile organoiodine and organobromine hydrocarbons in the Atlantic Ocean from 42°N to 72°S, Fresen. J. Anal. Chem., 359, 298–305, 1997.

Singh, H., Salas, L., and Stiles, R.: Methyl halides in and over the eastern Pacific (40° N–32° S), J. Geophys. Res., 88, 3684–3690, 1983.

Six, K. and Maier-Reimer, E.: Effects of plankton dynamics on seasonal carbon fluxes in an ocean general circulation model, Global Biogeochem. Cy., 10, 559–583, 1996.

Smythe-Wright, D., Boswell, S., Breithaupt, P., Davidson, R., Dimmer, C., and Eiras Diaz, L.: Methyl iodide production in the ocean: Implications for climate change, Global Biogeochem. Cy., 20, GB3003, doi:10.1029/2005GB002642, 2006.

Solomon, S., Garcia, R., and Ravishankara, A.: On the role of iodine in ozone depletion, J. Geophys. Res., 99, 20491–20499, 1994.

Stemmler, I., Rothe, M., Hense, I., and Hepach, H.: Numerical modelling of methyl iodide in the eastern tropical Atlantic, Biogeosciences, 10, 4211–4225, doi:10.5194/bg-10-4211-2013, 2013.

Tanzer, D. and Heumann, K.: Gas chromatographic trace-level determination of volatile organic sulfides and selenides and of methyl iodide in atlantic surface water, Int. J. Environ. Anal. Chem., 48, 17–31, 1992.

Toda, H. and Itoh, N.: Isolation and characterization of a gene encoding a S-adenosyl-L-methionine-dependent halide/thiol methyltransferase (HTMT) from the marine diatom Phaeodactylum tricornutum: Biogenic mechanism of CH_3I emissions in oceans, Phytochemistry, 72, 337–343, doi:10.1016/j.phytochem.2010.12.003, 2011.

Vogt, R., Sander, R., Von Glasow, R., and Crutzen, P.: Iodine chemistry and its role in halogen activation and ozone loss in the marine boundary layer: A model study, J. Atmos. Chem., 32, 375–395, 1999.

Wang, L., Moore, R., and Cullen, J.: Methyl iodide in the NW Atlantic: Spatial and seasonal variation, J. Geophys. Res.-Oceans, 114, C07007, doi:10.1029/2007JC004626, 2009.

Williams, J., Gros, V., Atlas, E., Maciejczyk, K., Batsaikhan, A., Schöler, H., Forster, C., Quack, B., Yassaa, N., Sander, R., and Van Dingenen, R.: Possible evidence for a connection between methyl iodide emissions and saharan dust, J. Geophys. Res.-Atmos., 112, D07302, doi:10.1029/2005JD006702, 2007.

Yokouchi, Y., Nojiri, Y., Barrie, L., Toom-Sauntry, D., and Fujinuma, Y.: Atmospheric methyl iodide: High correlation with surface seawater temperature and its implications on the sea-to-air flux, J. Geophys. Res.-Atmos., 106, 12661–12668, 2001.

Yokouchi, Y., Osada, K., Wada, M., Hasebe, F., Agama, M., Murakami, R., Mukai, H., Nojiri, Y., Inuzuka, Y., Toom-Sauntry, D., and Fraser, P.: Global distribution and seasonal concentration change of methyl iodide in the atmosphere, J. Geophys. Res.-Atmos., 113, D18311, doi:10.1029/2008JD009861, 2008.

Youn, D., Patten, K., Wuebbles, D., Lee, H., and So, S.-W.: Potential impact of iodinated replacement compounds CF3I and CH3I on atmospheric ozone: a three-dimensional modeling study, Atmos. Chem. Phys., 10, 10129–10144, doi:10.5194/acp-10-10129-2010, 2010.

Ziska, F., Quack, B., Abrahamsson, K., Archer, S. D., Atlas, E., Bell, T., Butler, J. H., Carpenter, L. J., Jones, C. E., Harris, N. R. P., Hepach, H., Heumann, K. G., Hughes, C., Kuss, J., Krüger, K., Liss, P., Moore, R. M., Orlikowska, A., Raimund, S., Reeves, C. E., Reifenhäuser, W., Robinson, A. D., Schall, C., Tanhua, T., Tegtmeier, S., Turner, S., Wang, L., Wallace, D., Williams, J., Yamamoto, H., Yvon-Lewis, S., and Yokouchi, Y.: Global sea-to-air flux climatology for bromoform, dibromomethane and methyl iodide, Atmos. Chem. Phys., 13, 8915–8934, doi:10.5194/acp-13-8915-2013, 2013.